Assessing vegetation condition in the presence of biomass burning smoke by applying the Aerosol-free Vegetation Index (AFRI) on MODIS images

E. BEN-ZE'EV†, A. KARNIELI*†, N. AGAM†, Y. KAUFMAN‡ and
B. HOLBEN‡

†The Remote Sensing Laboratory, Jacob Blaustein Institutes for Desert Research, Ben Gurion University of the Negev, Sede Boker Campus 84990, Israel
‡NASA/GSFC, Greenbelt, MD 20771, USA

Vegetation indices (VIs) such as the Normalized Difference Vegetation Index (NDVI) are widely used for assessing vegetation cover and condition. One of the NDVI's significant disadvantages is its sensitivity to aerosols in the atmosphere, hence several atmospherically resistant VIs were formulated using the difference in the radiance between the blue and the red spectral bands. The state-of-the-art atmospherically resistant VI, which is a standard Moderate Resolution Imaging Spectroradiometer (MODIS) product, together with the NDVI, is the Enhanced Vegetation Index (EVI). A different approach introduced the Aerosol-free Vegetation Index (AFRI) that is based on the correlation between the shortwave infrared (SWIR) and the visible red bands. The AFRI main advantage is in penetrating an opaque atmosphere influenced by biomass burning smoke, without the need for explicit correction for the aerosol effect. The objective of this research was to compare the performance of these three VIs under smoke conditions. The AFRI was applied to the 2.1 μm SWIR channel of the MODIS sensor onboard the Earth Observing System (EOS) Terra and Aqua satellites in order to assess its functionality on these imaging platforms. The AFRI performance was compared with those of NDVI and EVI. All VIs were calculated on images with and without present smoke, using the surface-reflectance MODIS product, for three case studies of fires in Arizona, California, and Zambia. The MODIS Fire Product was embedded on the images in order to identify the exact location of the active fires. Although good correlations were observed between all VIs in the absence of smoke (in the Arizona case $R^2=0.86$, 0.77, 0.88 for the NDVI–EVI, AFRI–EVI, and AFRI–NDVI, respectively) under smoke conditions a high correlation was maintained between the NDVI and the EVI, while low correlations were found for the AFRI–EVI and AFRI–NDVI (0.21 and 0.16, for the Arizona case, respectively). A time series of MODIS images recorded over Zambia during the summer of 2000 was tested and showed high NDVI fluctuations during the study period due to oscillations in aerosol optical thickness values despite application of aerosol corrections on the images. In contrast, the AFRI showed smoother variations and managed to better assess the vegetation condition. It is concluded that, beneath the biomass burning smoke, the AFRI is more effective than the EVI in observing the vegetation conditions.

*Corresponding author. Email: karnieli@bgu.ac.il

1. Introduction

The spectral properties of vegetated areas present different mixtures of vegetation, soil brightness, environmental effects, shadow, soil colour, moisture, etc. (Tucker 1979, Huete 1987, Bannari *et al.* 1995). Dozens of vegetation indices (VIs) have been developed during the past decades in order to assess the state of vegetation qualitatively and quantitatively. The most widely used VI is the Normalized Difference Vegetation Index (NDVI) (Rouse *et al.* 1974):

$$\mathrm{NDVI} = (\rho_{\mathrm{NIR}} - \rho_{\mathrm{red}})/(\rho_{\mathrm{NIR}} + \rho_{\mathrm{red}}) \tag{1}$$

where ρ_{NIR} and ρ_{red}, are the reflectance in the near-infrared (NIR) and red channels, respectively. Although this index is used extensively, it has a few weaknesses. First, it is sensitive to the effects of soil background (type, brightness, colour, wetness, etc.). For overcoming this issue Huete (1987) invented the Soil Adjusted Vegetation Index (SAVI). The other weakness is due to the presence of light-absorbing and scattering aerosols in the atmosphere (Kaufman and Tanré 1992). This weakness causes some complexities in calculating true vegetation values in an atmosphere contaminated by different types of aerosols such as biomass burning smoke, volcanic ash, industrial emissions, dust, etc. (Slater and Jackson 1982, Kaufman 1989, Kaufman and Tanré 1996). Spatial and temporal studies carried out using airborne and space-borne images have shown the effect of the atmosphere on vegetation indices (Kaufman and Sendra 1988, Qi *et al.* 1993, Bannari *et al.* 1995, King *et al.* 1999, Karnieli *et al.* 2001). As a result, Kaufman and Tanré (1992) examined two VIs that directly correct the red radiance for aerosol effect by incorporating the blue band. These are the Atmospheric Resistant Vegetation Index (ARVI) and the Atmospheric Resistant SAVI (SARVI). Recently the Enhanced Vegetation Index (EVI) was developed in order to optimize the vegetation signal with improved sensitivity in high biomass regions and improved vegetation monitoring while correcting for canopy background signals reducing atmosphere influences. The EVI is based on the NDVI, SAVI, and ARVI indices, and uses functionalities from each one of them in order to overcome the soil and the atmosphere interferences. EVI is formulated as:

$$\mathrm{EVI} = G \frac{\rho_{\mathrm{NIR}} - \rho_{\mathrm{red}}}{\rho_{\mathrm{NIR}} + C1\rho_{\mathrm{red}} - C2\rho_{\mathrm{blue}} + L} \tag{2}$$

where $G=2.5$, $C_1=6$, $C_2=7.5$, and $L=1$. This index was recently used and its capability to penetrate forest fire smoke plum was demonstrated by Huete *et al.* (1999, http://eospso.gsfc.nasa.gov/ftp_ATBD/REVIEW/MODIS/ATBD-MOD-13/atbd-mod-13.pdf).

A different approach for assessing the surface cover in the absence of aerosol effect relies on VIs that are based on the shortwave infrared (SWIR) spectral bands (Kaufman and Remer 1994, Miura *et al.* 1998). Following this approach, the current study analyses a new SWIR-based index, named the Aerosol-free Vegetation Index (AFRI) (Karnieli *et al.* 2001). AFRI uses the 2.1 μm band due to the following reasons.

- Its location is in one of the atmospheric windows and therefore it is less influenced by atmospheric gases such as O_2, O_3, H_2O, CO_2, etc.
- Its location is relatively far from the Earth's peak emission at about 10 μm, and thus, in contrast to the 3.75 μm band (Holben *et al.* 2002), it is not affected by uncertainties in the correction of emitted radiation.

- The 2.1 μm band is much longer than the size of the most common types of aerosols, such as smoke or sulphates (but not larger than dust), and consequently penetrates the atmospheric column in presence of these aerosols (Kaufman and Remer 1994).
- Bio-physiological speaking, as chlorophyll absorption by healthy vegetation tends to reduce the reflectivity in the visible portion of the electromagnetic spectrum, liquid water in the plants, associated with the presence of chlorophyll, absorbs radiation in the 2.1 μm region.
- Similarly, factors that reduce reflectivity of soils in the visible region, such as soil moisture or self-shadow, act in the same direction in the SWIR region as well.

The AFRI index was tested during a field campaign that was carried out in 1997 in Israel. Several instruments were installed on a light aircraft, which flew at an altitude of 300 m, an altitude low enough to minimize the atmospheric affect. Under clear sky conditions, the field spectrometer (Analytical Spectral Devices, ASD) measurements revealed a high correlation between the SWIR 2.1 μm spectral band and the red spectral bands with a general linear relationship of:

$$\rho_{0.645} = 0.5\rho_{2.1} \tag{3}$$

where $\rho_{0.645}$ and $\rho_{2.1}$ are the reflectance of the red band and the SWIR band, respectively. Introducing equation (3) into equation (1) yields:

$$\text{AFRI} = (\rho_{\text{NIR}} - 0.5\rho_{2.1})/(\rho_{\text{NIR}} + 0.5\rho_{2.1}) \tag{4}$$

Similar to other vegetation indices such as NDVI and EVI, AFRI was proven to be sensitive to the green, photosynthetically active vegetation, though by sensing the liquid water content instead of the chlorophyll absorption in the red bands. This is since photosynthetically active vegetation has to have high liquid water content. However, as noted, AFRI's main advantage is its ability to penetrate an atmosphere opaque by biomass burning aerosols, and consequently producing a realistic vegetation condition image. According to Karnieli *et al.* (2001) under clear sky conditions the AFRI closely resembles the NDVI. The values of both indices are almost identical and thus it is possible to assess vegetation conditions without using the visible bands that are more sensitive to atmospheric scattering.

The AFRI index was previously tested on an image of Cuiábá, Brazil, taken during the Smoke Clouds and Radiation–Brazil (SCAR-B) experiment by the airborne hyperspectral imager—Airborne Visible/Infrared Imaging Spectrometer (AVIRIS) onboard a NASA ER-2 aircraft. The ER-2 flew at an altitude of 20 km while the AVIRIS acquired images with a 20 m spatial resolution at nadir and a 10 km swath width. Implementation of the AFRI on the image gave near true vegetation values for the vegetated area covered by biomass burning smoke (Karnieli *et al.* 2001). Recently, AFRI, applying the 1.6 μm channel of the SPOT-VEGETATION, was tested under different optical depth conditions over Taiwan (Liu *et al.* 2004). It was concluded that the AFRI and ARVI performed better than the NDVI.

The objective of this work is to continue the exploration of the AFRI by assessing the functionality of satellite sensors such as Moderate Resolution Imaging Spectrometer (MODIS), and its ability to serve as an imaging platform for the use of the AFRI.

2. Data sources and case studies

2.1 *Satellite sensor data*

The MODIS instruments onboard the Earth Observing System (EOS) Terra and Aqua satellites provide high radiometric sensitivity (12 bit) in 36 spectral bands ranging in wavelength from 0.4 to 14.4 μm. Two bands are imaged at a nominal resolution of 250 m at nadir, five bands at 500 m, and the remaining 29 bands at 1000 m.

2.1.1 MODIS products. There are 44 standard MODIS data products in use for studying global change. These products are being used in a variety of disciplines, including oceanography, biology, and atmospheric science. Currently, the products have two main versions, V3 and V4. The latter is a newer version and is used in most of the cases. Four different products are used in this research.

MOD02_L1b. The Level 1B dataset contains calibrated and geolocated at-aperture radiances for 36 bands generated from MODIS Level 1A sensor counts (MOD01). In addition, Earth bidirectional reflectance distribution function (BRDF) may be determined for the solar reflective bands (1–19, 26) through knowledge of the solar irradiance (e.g. determined from MODIS solar-diffuser data, and from the target–illumination geometry). Additional data including quality flags, error estimates, and calibration, can be found in Isaacman (2002), Toller and Isaacman (2002), and in the MODIS web site at http://modis.gsfc.nasa.gov/data/dataproducts.php?MOD_NUMBER=02.

MOD04_L2—Aerosol Product. The MODIS Aerosol Product monitors the ambient aerosol optical thickness over the oceans globally and over a portion of the continents. Furthermore, the aerosol size distribution is derived over the oceans, and the aerosol type is derived over the continents. Daily Level 2 data are produced at the spatial resolution of 10 km × 10 km (at nadir). The product is used to study aerosol climatology, sources and sinks of specific aerosol types (e.g. sulphates and biomass-burning aerosol), interaction of aerosols with clouds, and atmospheric corrections of remotely sensed surface reflectance over the land. Information about this product can be found at the MODIS web site (http://modis.gsfc.nasa.gov/data/dataproducts.php?MOD_NUMBER=04). The products disadvantage in this research was its low spatial resolution of 10 km × 10 km.

MOD09—Surface Reflectance. The MODIS Surface-Reflectance Product (MOD09) is computed from the MODIS Level 1B land bands 1, 2, 3, 4, 5, 6, and 7 (centred at 0.648, 0.858, 0.47, 0.55, 1.24, 1.64, and 2.13 μm, respectively). The product is an estimate of the surface spectral reflectance for each band, corrected for atmospheric scattering and absorption by atmospheric gases and aerosols. The images are in Integerized Sinusoidal projection, WGS 84 Datum. NASA offers different MOD09 products, depending on resolution and an eight-day cloud screened product. This research used the daily MOD09GHK (Gridded Half Kilometer) and the MOD09A1 (eight-day) 1 km products. Further information can be found at http://modis.gsfc.nasa.gov/data/dataproducts.php?MOD_NUMBER=09. The surface reflectance products do not manage to fully 'clear' the biomass burning aerosols from the images (Vermote *et al.* 2002), nor did they manage in this research.

MOD14—Thermal Anomalies—Fires and Biomass Burning. The MODIS Thermal Anomalies product includes fire occurrence (day/night), fire location, the logical criteria used for the fire selection, and an energy calculation for each fire. The

product also includes composite eight-day-and-night fire occurrence, composite monthly day-and-night fire occurrence, gridded 10 km summary per fire class (daily/eight-day/monthly), and a gridded 0.5° summary of fire counts per class (daily/eight-day/monthly). The Level 2 product includes various fire related parameters including the occurrence of day and night-time thermal anomalies, flagged and grouped into different temperature classes with emitted energy from the fire. These parameters are retrieved daily at 1 km resolution and can be viewed in the MODIS web site (http://modis.gsfc.nasa.gov/data/dataproducts.php?MOD_NUMBER=14), with additional reading in Justice *et al.* (2002).

2.2 *Datasets*

This section sums up three web-based sites for locating biomass burnings. These databases also offer visual and textual (tables and graphs) data from different areas of the world with natural and anthropogenic fires.

2.2.1 GBA2000. The Global Burnt Area 2000 Initiative (GBA2000) web site (http://www.grid.unep.ch/activities/earlywarning/preview/ims/gba/test.htm) is an initiative launched by the Global Vegetation Monitoring (GVM) Unit of the Joint Research Center—European Committee (JRC), in partnership with six other institutions, with the specific objective being to produce a map of the areas burnt globally for the year 2000, using the medium resolution (1 km) satellite imagery provided by the SPOT-VGT system, and to derive statistics of area burnt per type of vegetation cover. The web site offers an interactive global map for the year 2000 with different layers (borders, trees, land covers, etc.), statistical tabular and graph data, and downloadable geographic information system (GIS) (ArcInfo) and ENVI/ERDAS layers.

2.2.2 Earth Observatory. NASA's Earth Observatory (EO) web site (http://earthobservatory.nasa.gov) presents different remote sensing features. The 'Natural Hazards' section is devoted to satellite images of natural and anthropogenic disasters as fires, volcano eruptions, floods, etc. The fire section has many images of fires around the world, most taken by the MODIS instrument. Using this site makes it easier on the user in finding specific images due to the fact that all the images have thumbnails and so one can evaluate the image before downloading it.

Due to AFRI's sensitivity to waterbodies (NIR and SWIR wavelengths are almost totally absorbed by water) and its purpose of stating vegetation condition through smoke, vast vegetated areas with as minimum clouds and waterbodies as possible were explored through this web site.

2.2.3 SAFARI2000. The Southern African Regional Science Initiative (SAFARI2000) was an international science research campaign during the dry season of the millennium. SAFARI2000 was aimed at developing a better understanding of the southern African atmosphere. It included atmospheric research of biomass-burning aerosols from large fires (natural and anthropogenic) in different countries in the south of the African continent. The project combined space-borne, airborne, and ground measurement stations, which measured aerosol characteristics and behaviour. The SAFARI2000 ground-based aerosol measurements were conducted with several sunphotometers, which are part of the AErosol RObotic NETwork (http://aeronet.gsfc.nasa.gov/). The goal of the program was to

assess aerosol optical properties and validate satellite retrievals of aerosol optical properties.

The first and last databases (i.e. GBA2000 and SAFARI2000) have much data but cannot tell of the satellite coverage. Therefore, NASA's EO was found to be the most sufficient of the three due to the visualization of the images. One must first find the images, which fit most for the research, and only then, data concerning vegetation coverage, smoke emission, aerosol optical thickness (AOT) etc., can be downloaded and used.

2.3 *Case studies*

2.3.1 Rodeo—Chediski. The Rodeo–Chediski fire burned in east-central Arizona from 18 June 2002 and was not controlled until 7 July. It was the worst forest fire in Arizona to date, consuming aproximetly $1890 \, km^2$ of woodland. Initially there were two separate fires. The first fire, the Rodeo fire, was reported on the afternoon of 18 June near the Rodeo Fairgrounds on the Fort Apache Reservation (http://www.wikipedia.org/wiki/Rodeo-Chediski_fire).

MODIS L1B images of the region were downloaded from NASA's EOS Distributed Active Archive Center (DAAC) web site (http://edcimswww.cr.usgs.gov/pub/imswelcome/plain.html). The two main weaknesses of the L1B images in this research are the cloud cover and the fact that the images are not atmospherically corrected, thus the pixel values are not true-ground values but top-of-atmosphere (TOA)-sensor values, known as apparent reflectance. Due to this weakness, the red–SWIR ratio cannot be computed truthfully; therefore the AFRI could not be employed. Hence, the L1B images were used, as reference images in order to monitor the daily expansion of the fire and the smoke but NDVI or AFRI were not calculated on them.

The MODIS surface reflectance product (MOD09) was used in order to evaluate the accurate ground reflectance. Two surface reflectance products were downloaded from the EOS DAAC web site: MOD09GHK, and MOD09A1. Both products are atmospherical corrected (gas absorption and molecular and aerosol scattering). The former is a daily 500 m restructured version of its primary input MOD09_L2, while the latter is a 1 km eight-day composite of the gridded level-2 surface reflectance product. A 12-day (day of the year—date) archive was built with the daily images denoted as 2002161–2002185 (10 June–4 July 2002). In order to compute the red–SWIR ratio, reflectance was calculated for a clear-day image (10 June) of the Rodeo–Chediski region. A vegetative area of $3360 \, km^2$ was chosen and saved as an area of interest (AOI). Correlation was computed for the red and SWIR $(2.1 \, \mu m)$ bands.

Subsequently, a cross-section was drawn over an area of vegetation over the region of the expected fire and smoke. This procedure was performed on all the images during the time period. Figure 1 shows the subset and cross-section of an image recorded a day after the fire started. The cross-section's pixel values were extracted and NDVI, EVI, and AFRI were calculated for each pixel. Two daily subseted images, dating 10 and 19 June 2000, i.e. eight days before, and a day after the fire started, were used in order to examine the behaviour of the indices, with and without the presence of smoke.

Two MODIS products were used for verifying the fire and smoke. A fire product (MOD14) was layered on the image showing the exact location of the active fire and the aerosol product (MOD04) was used in order to monitor the expansion and
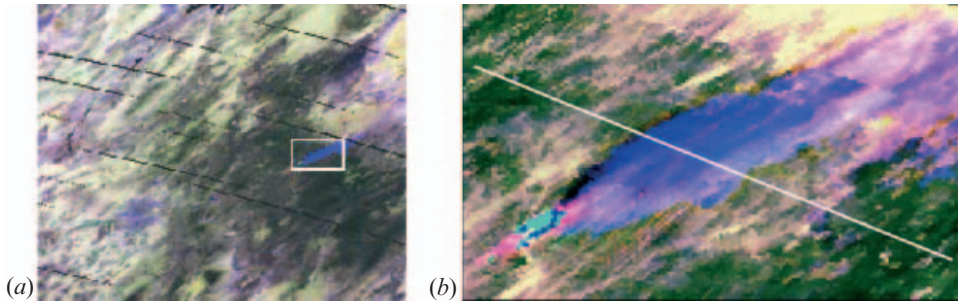
Figure 1. (*a*) A false-colour (RGB=2.13, 0.865, 0.47 μm) daily surface reflectance image of the Rodeo–Chediski region. The forest is seen in dark green. The white rectangle boxes the fire and smoke and is enlarged in (*b*). (*b*) A subset of (*a*). The fire can be seen in a light-blue hue, the burn scars are pink, and the smoke dark blue/purple. NDVI and AFRI values were calculated for the cross-section.

movement of the biomass burning smoke, and to differentiate it from clouds, although it was not layered on the images due to its low resolution (10 km × 10 km).

2.3.2 California. Late season fires were burning in the Sierra Nevada Mountains in California during the summer of 2002. The area is mainly vegetated by mountain coniferous forest communities, which cover the Sierra Nevada Mountains. The community is a mixture of conifers dominated by Ponderosa pine, with some incense-cedar and California Black Oak at lower elevations and increasing numbers of sugar pine and white fir at the higher elevations (http://biology.usgs.gov/s+t/ SNT/noframe/cal63.htm). Figure 2 is an Aqua–MODIS image taken on 25 November 2002. The figure shows these and other fires scattered across the state, and what could be a mixture of smoke and urban air pollution which is nestled into the San Joaquin Valley (http://earthobservatory.nasa.gov).

Daily surface reflectance (MOD09GHK) images of the North American continent covering the area of California were downloaded for the dates 10–30 November 2003. Due to cloud cover over the region a single fire (1202446.40W/ 384501.79N), which was visible during several days, was chosen and subseted from all the images (figure 3(*a*)).

2.3.3 Mongu, Zambia. After reviewing the statistics in the GBA2000 web site and in conjunction with SAFARI2000, two more regions were found suitable for the research, Zambia and Mozambique. Both countries showed among the largest burnt areas in the African continent, for the given dry season (August–September). Mozambique suffered an average loss of roughly $32\,500\,\text{km}^2$ each month while Zambia experienced a 'slow start' with $15\,988\,\text{km}^2$ of burnt territory in August, and a rise by more than 100% to $33\,180\,\text{km}^2$ during September (http://www.grid.unep.ch/ activities/earlywarning/preview/ims/gba/test.htm). Zambia was chosen from the two countries as a case study due to the fact that it participated in the SAFARI2000 campaign and thus ground measurements were obtained during the summer months, and may help in confirming and measuring the source and quantities of the aerosols in the images. During the SAFARI2000 campaign, three AERONET sites were operational in Zambia: Mongu (15° S, 23° E), Senanga (16° S, 23° E), and Ndola (12° S, 28° E). Mongu was chosen as the primary site due to its highest monthly average of biomass burning smoke. Relatively high AOT AERONET-measurements (AOT_{500}=1.78) were measured during 15 September (http://
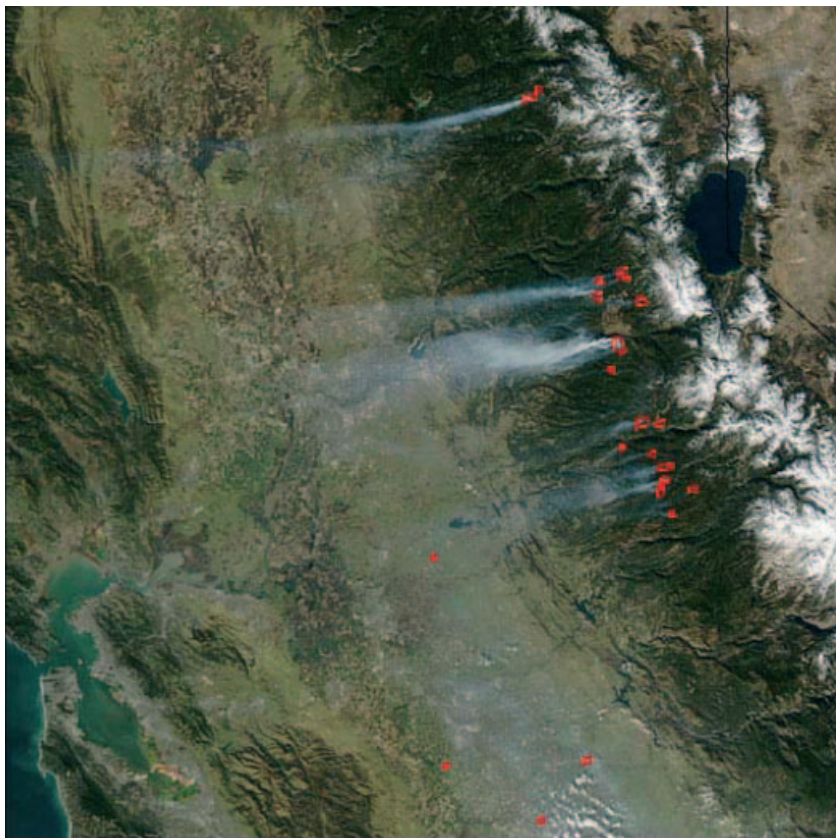
Figure 2. An Aqua–MODIS true-colour image of fires (red outlines) burning in California. At the upper right is Lake Tahoe, on the California–Nevada border. At the lower left is San Francisco Bay. Big plumes of smoke stream westward from the fires that are burning in the Sierra Nevada Mountains.

aeronet.gsfc.nasa.gov/). This certain event was chosen and analysed using images taken during August and September.

The principal vegetative cover in western Zambia is Miombo woodland savannah, with some grassland savannah, cropland, and seasonal marshes in the river floodplains. Grasses growing between the Miombo trees account for much of the biomass fuel burned in the woodland savannah regions (Eck *et al.* 2001).

All three case studies were carried out *in silico* and no true ground measurements were performed.

3. Analysis and results

3.1 *Rodeo–Chediski*

The biomass burning smoke of the Rodeo–Chediski fire blew over the forest in a linear fashion. Thus AFRI could be calculated over a cross-section transecting the smoke and the surrounding vegetation. The red–$SWIR_{2.1}$ ratio was calculated for a vegetated area on a clear day (10 June 2002) and showed high linear correlation of $R^2 = 0.96$ (figure 4). This significant result is consistent with previous findings
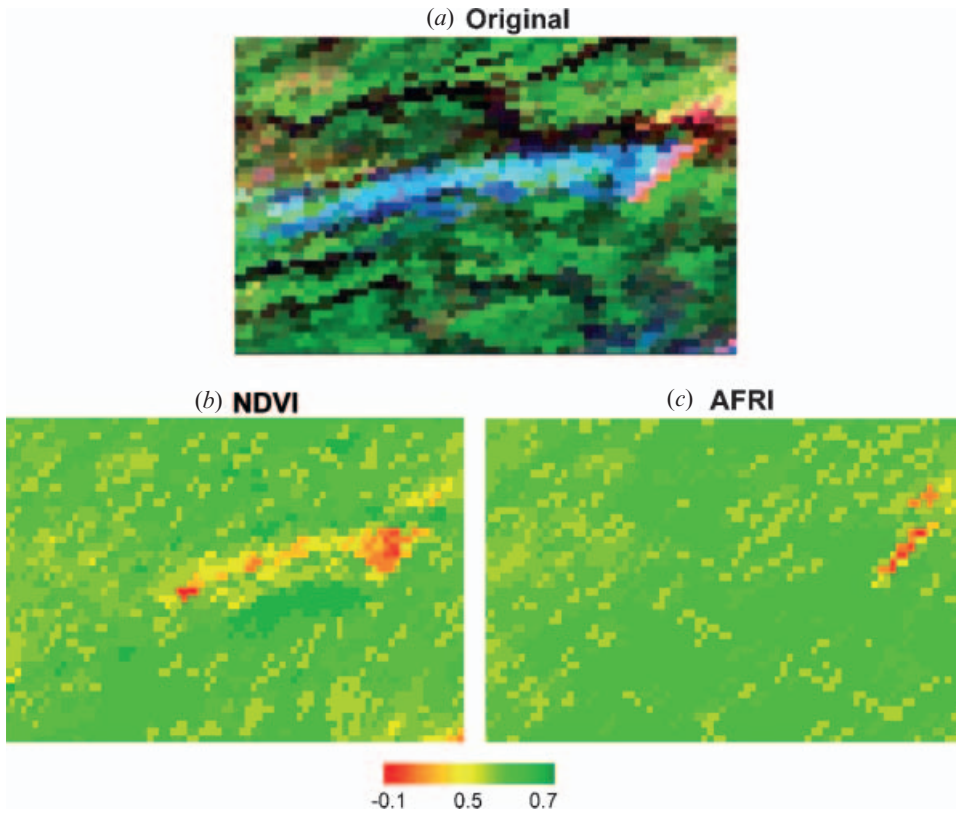
Figure 3. (*a*) A false-colour (RGB=2.13, 0.865, 0.47 μm) image of the fire chosen in the California mountains. The vegetation is green, the active fire is seen in red, and the smoke is blue. (*b*) A pseudo-colour NDVI image. The smoke can be seen in yellow and red colours. (*c*) A pseudo-colour AFRI image. The smoke is transparent and thus the vegetation underneath is seen. The active fire can be seen due to the 2.1 μm wavelength's proximity to the thermal emission peak of the fire.

(Kaufman *et al*. 1997a, 2000, Miura *et al*. 1998, King *et al*. 1999, Karnieli *et al*. 2001) and is the base for using the AFRI.

Figure 5 represents correlations between the different VIs before and during the fire. For the cross-section pixels in the image dating eight days before the fire started, high correlations were found between the NDVI and EVI (R^2=0.86), AFRI and EVI (R^2=0.77), and AFRI and NDVI (R^2=0.88). This indicates that prior to the fire, the AFRI showed a similar trend as the NDVI and EVI over vegetated areas. AFRI and NDVI have almost identical values as noted before by Karnieli *et al*. (2001). The AFRI and NDVI values were found to have higher values than the EVI (Huete *et al*. 2002, Ferreira *et al*. 2004). Scatter plots of the same pixels for the day after the fire started present two scatters—one of the smoke-free area and the other of the smoky area itself. Correlations among the VIs outside the smoky area remain relatively high, but obviously the two clusters cannot be connected. It is interesting to note the relatively high correlation (R^2=0.73) between NDVI and EVI over the smoke, which demonstrates the disability of the EVI, similar to the NDVI, to detect the vegetation through an opaque atmosphere.

Figure 6(*a*) shows the NDVI, EVI, and AFRI values along the cross-section eight days before the fire started. Similar trend of the VIs can be noticed. The AFRI
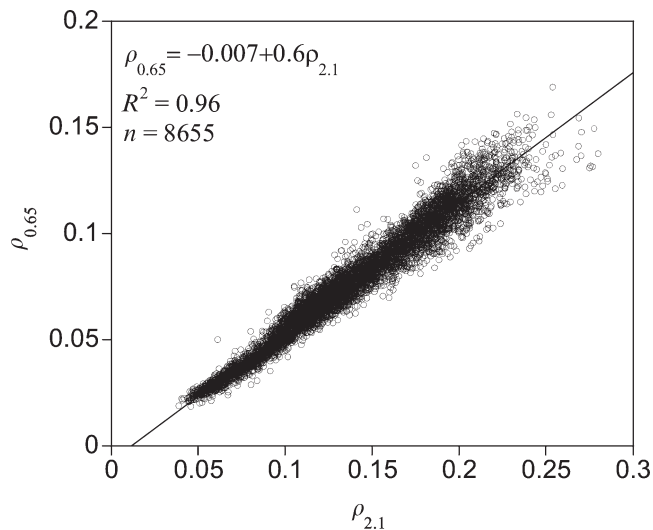
Figure 4. A scatter plot of the reflectance in the red and SWIR band for a vegetated area in the Rodeo–Chediski region. Note the high correlation between the two bands.

values are very similar to those of the NDVI, while the EVI has a similar trend but much lower values. Figure 6(*b*) shows the same VIs along the same cross-section one day after the fire outburst. One may note the similarity of the AFRI and NDVI values over the vegetated areas (both ends of the graph) and the significant decrease in NDVI values within the smoke contaminated area, while the AFRI maintains its high values throughout the entire cross-section. The EVI mimics both indices along the vegetated smoke-free pixels (although with lower values) and is also affected by the smoke, although to lesser degree than the NDVI.

In addition, AFRI and NDVI were computed on the whole sub-image over the fire and vicinity. Figure 7 shows both NDVI and AFRI pseudo-colour images. The vegetation can be seen in green hues, the soil is yellow and orange, and the smoke is red. One may note the smoke covering the vegetation in the NDVI image (figure 7(*a*)); however, in figure 7(*b*) the AFRI manages to penetrate through the smoke, and thus expected vegetation values are calculated. The active fire can be seen in the AFRI image as dark green due to the proximity of the SWIR band to the thermal emission. Furthermore, a red streak, similar to the smoke in the NDVI image, can be seen stretching from the fire outward. This is not smoke but the shadow of the smoke as can be seen in figure 1(*b*). Note that this shadow also affects AFRI values along the cross-section (figure 6).

3.2 *California*

The fire used in this case study was too small and did not emit a high enough concentration of smoke in order to be monitored and tested during its period of burning. Thus, a single day (25 November 2002) was chosen, when the fire emitted the highest concentration of smoke that covered the largest vegetated area. NDVI and AFRI were calculated from the surface reflectance (MOD09GHK) values in the subseted image of the fire region. The NDVI, as suspected, did not manage to penetrate the smoke and showed very low values in its presence. The AFRI, on the other hand, pierced through the biomass burning aerosols and managed to calculate
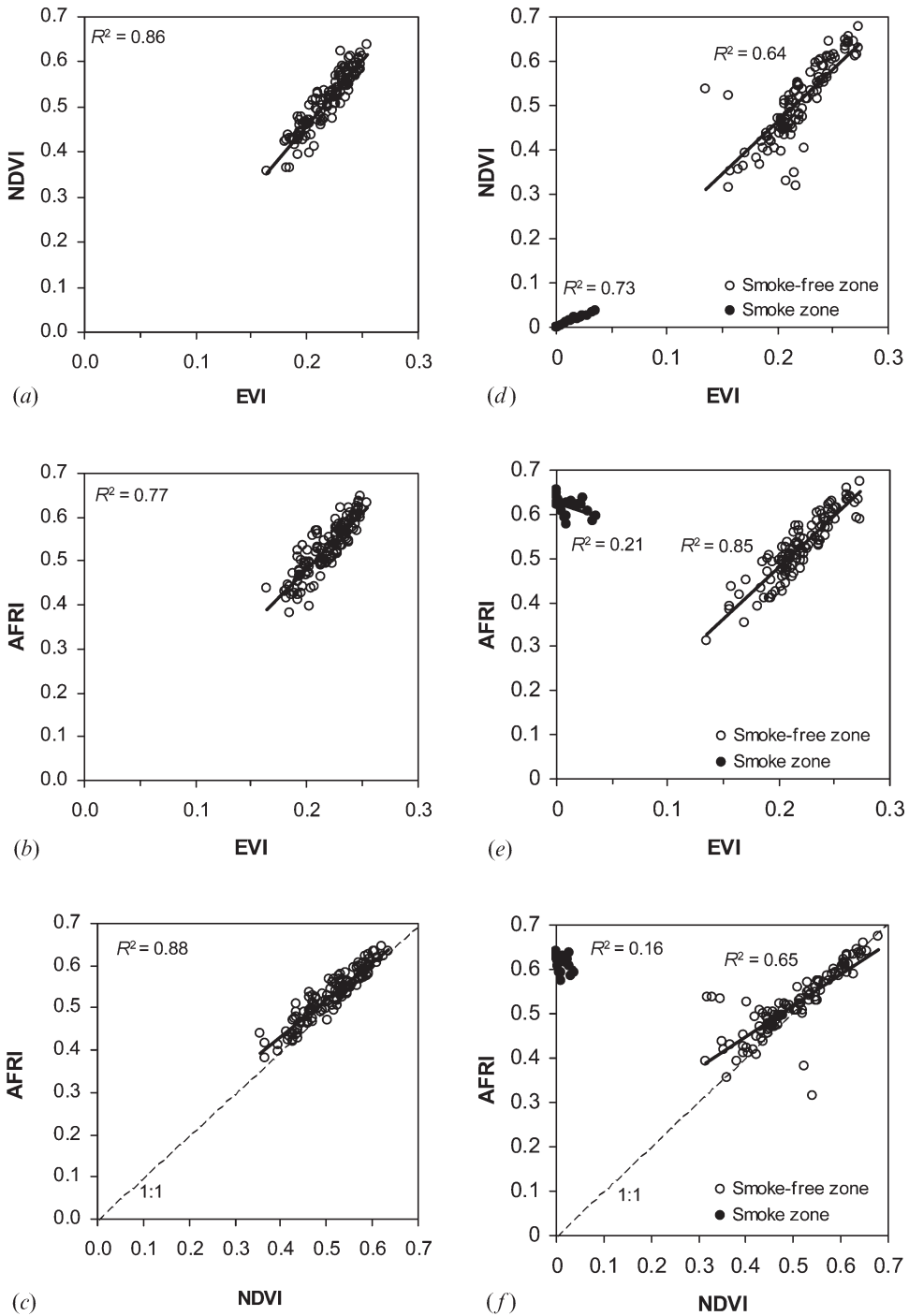
Figure 5. Correlations between the different VIs before and during the fire for the Rodeo–Chediski case study: (*a*) NDVI vs EVI before fire; (*b*) AFRI vs EVI before fire; (*c*) AFRI vs NDVI before fire; (*d*) NDVI vs EVI during fire; (*e*) AFRI vs EVI during fire; and (*f*) AFRI vs NDVI during fire.
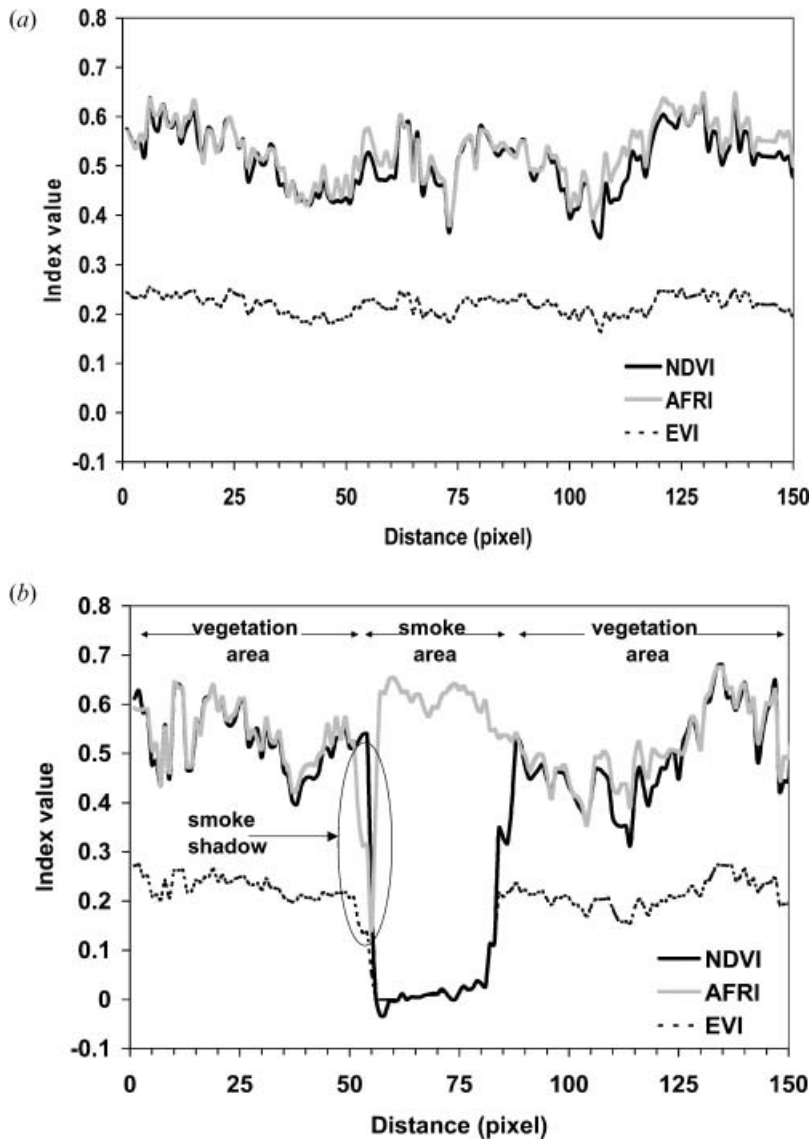
Figure 6. NDVI, EVI and AFRI values along the cross-section embedded on the image before and after the fire broke out: (*a*) dating 10 June; one may note the resemblance between the AFRI and NDVI. EVI shows a similar trend though with fewer fluctuations and lower values; and (*b*) dating a day after the fire started (19 June); NDVI and EVI values drop during the smoke contaminated pixels, while the AFRI manages to keep its high values. Note the decrease in AFRI values due to the smoke's shadow.

and illustrate near true vegetation condition values. Figure 3(*b*) and (*c*) shows the NDVI and AFRI subseted images of the fire.

3.3 *Mongu*

The bush fires overcasting the vegetated area in Zambia are indicated by fluctuations of AOT_{500}, ranging between 0.15 and 1.78. In a different manner than
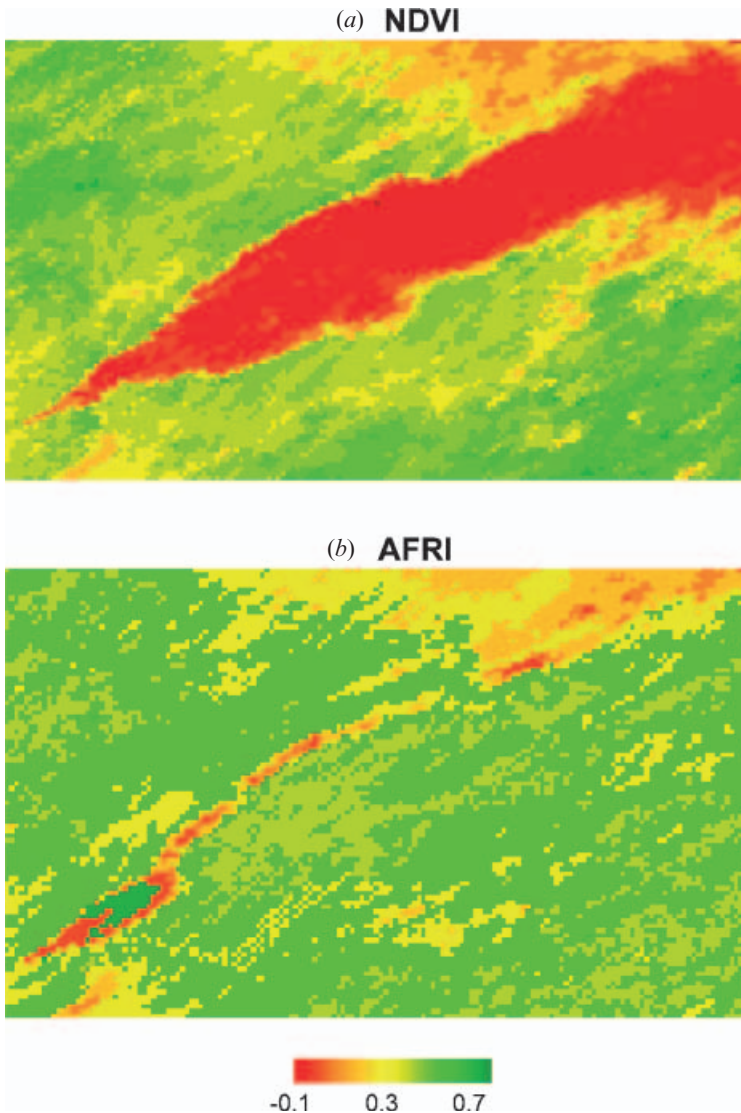
Figure 7. Pseudo-colour images of the Rodeo–Chediski fire. The images were calculated from the surface reflectance (MOD09GHK) image dating 19 June 2002: (*a*) NDVI; and (*b*) AFRI.

the forest fire cases described above, the current smoke was widely spread over the entire region, thus identifying the active fires was impossible. Therefore, in order to demonstrate the capability of the proposed index, a cross-section (approximately 80 km long) was stretched over the vegetated area. Spatial averages of the NDVI and AFRI were computed and embedded in a time series along with AOT_{500} values (table 1, figure 8). The descriptive statistics computed for these data are presented in table 2. It can be seen that the averages of the NDVI and the AFRI are very similar. Moreover, a general look at figure 8 reveals similar trends of both indices. However, a careful examination of figure 8 implies that during dates characterized by high values of AOT_{500}, the AFRI maintained relatively constant values, while

Table 1. NDVI and AFRI values of the cross-section over a vegetated area near Mongu, Zambia, dating 1 August–27 September 2000 (day of year). 'N/A' represents dates with no images or images where the cross-section is in between orbits and there are no data. The AOT_{500} values are averaged daily values from the AERONET site in Mongu.

Year/DOY*	NDVI	AFRI	AOT_{500}
2000/214	0.689762	0.681254	0.364
2000/215	0.635174	0.631853	0.519
2000/216	0.660839	0.658198	0.392
2000/217	0.649002	0.646316	0.221
2000/218	0.623015	0.622381	0.189
2000/219	N/A	N/A	0.2
2000/220	N/A	N/A	0.206
2000/221	N/A	N/A	0.201
2000/222	N/A	N/A	0.151
2000/223	N/A	N/A	0.244
2000/224	N/A	N/A	0.217
2000/225	N/A	N/A	0.219
2000/226	N/A	N/A	0.36
2000/227	N/A	N/A	0.179
2000/228	N/A	N/A	0.205
2000/229	N/A	N/A	0.166
2000/230	N/A	N/A	0.222
2000/231	N/A	N/A	0.337
2000/232	0.580309	0.687744	0.429
2000/233	0.660501	0.653751	0.65
2000/234	0.602838	0.60043	0.585
2000/235	cloudy	cloudy	0.752
2000/236	0.692186	0.687233	0.36
2000/237	0.608708	0.605597	0.399
2000/238	0.665724	0.66289	0.242
2000/239	0.627113	0.623621	0.291
2000/240	0.628632	0.625597	0.221
2000/241	0.644653	0.64094	0.235
2000/242	0.590558	0.588306	0.187
2000/243	0.570435	0.56984	0.208
2000/244	N/A	N/A	0.391
2000/245	0.515711	0.643366	0.561
2000/246	clouds	clouds	0.737
2000/247	clouds	clouds	1.131
2000/248	0.515711	0.643366	1.492
2000/249	0.620485	0.616786	1.475
2000/250	0.483257	0.593902	1.37
2000/251	N/A	N/A	1.182
2000/252	0.58078	0.578963	1.369
2000/253	clouds	clouds	1.344
2000/254	0.638876	0.636679	0.873
2000/255	0.598183	0.596704	0.412
2000/256	0.624526	0.620826	0.676
2000/257	0.651968	0.645184	0.448
2000/258	0.509227	0.573906	0.848
2000/259	clouds	clouds	1.782
2000/260	N/A	N/A	1.341
2000/261	0.614681	0.614653	1.364
2000/262	clouds	clouds	N/A
2000/263	0.664719	0.658506	1.014
2000/264	0.190085	0.667984	0.987
2000/265	0.610753	0.609924	0.418

Table 1. (*Continued.*)

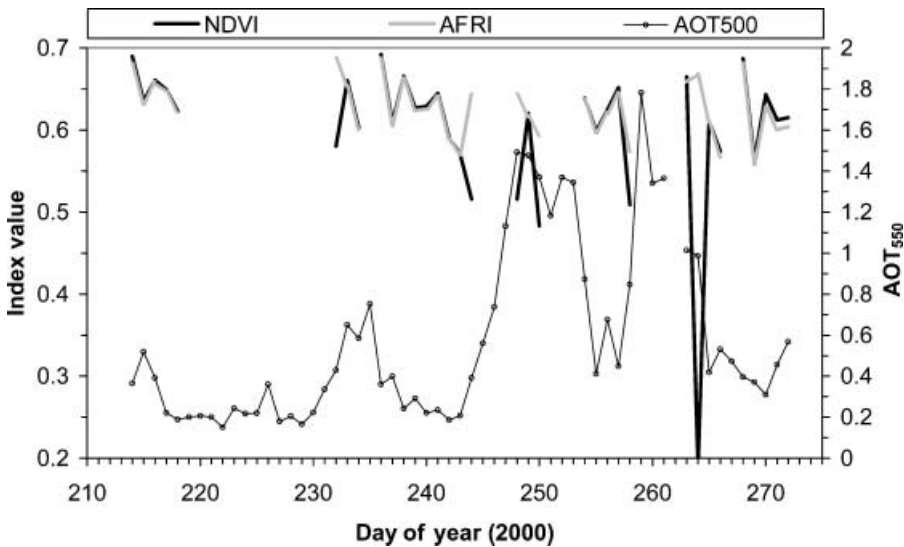| Year/DOY*	NDVI	AFRI	AOT_{500}
2000/266	0.573887	0.5673	0.53
2000/267	N/A	N/A	0.473
2000/268	0.687004	0.681331	0.396
2000/269	0.563614	0.558002	0.371
2000/270	0.643015	0.627992	0.309
2000/271	0.612275	0.600287	0.456
2000/272	0.615309	0.604497	0.568

*DOY=day of year

Figure 8. NDVI, AFRI, and AOT_{500} values over Zambia during a two months period (August–September 2000). Note the similar tendency of the NDVI and the AFRI. Nevertheless, the former is perturbed by the increase in smoke, which is noted by the high AOT_{500} values, while the latter is less influenced by the smoke and maintains a more stable tendency.

remarkable fluctuations in the NDVI values are observed. These fluctuations are well expressed as relatively high standard deviation of NDVI (0.09) compared to that of AFRI (0.04). In order to verify that the smoke significantly affects NDVI (but not AFRI) the computed values of both indices were plotted against the AOT_{500} (figure 9). Although the meaningless correlations, the slope of the NDVI

Table 2. Descriptive statistics of the NDVI and AFRI values computed from the data presented in table 1.

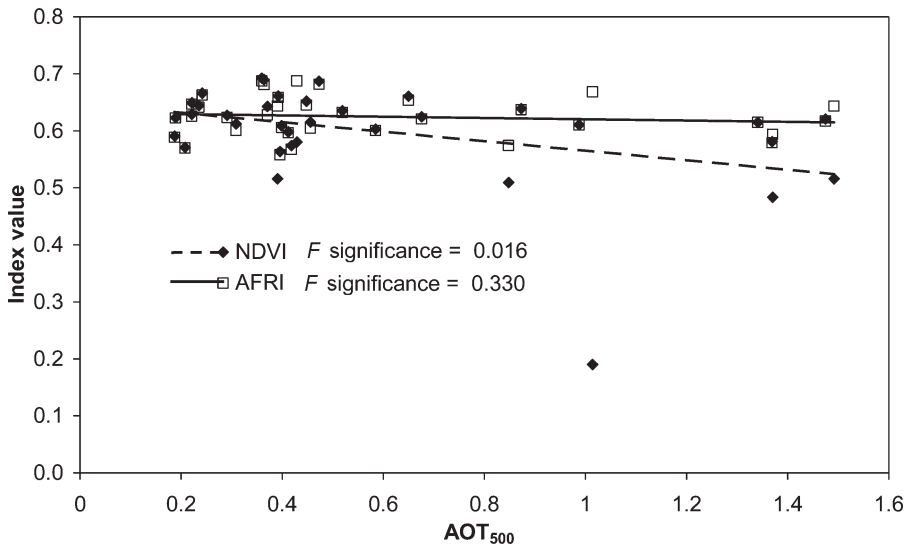|	NDVI	AFRI
Average	0.599	0.625
Standard deviation	0.087	0.035
Maximum	0.692	0.688
Minimum	0.190	0.558
Range	0.502	0.130

E. Ben-Ze'ev et al.

Figure 9. NDVI and AFRI as a function of AOT_{500}. Note that although correlations are meaningless, the slope of the NDVI was found to be significantly different from zero and the AFRI not.

was found to be significantly different from zero (*F* significance was computed to be 0.016), while the slope of the AFRI was not (*F* significance equal 0.33). It can, therefore, be confidently concluded that while NDVI is affected by smoke, AFRI is not.

4. Discussion

AFRI was originally formulated with data obtained from an extremely low altitude aircraft flight (300 m) and tested on an AVIRIS image taken from a height of 20 km, with a spatial resolution of 20 m (Karnieli *et al.* 2001). Its success, together with the available data from satellite images, led to this upscaling research in which the AFRI was tested using data obtained from the space-borne level on moderate-resolution satellite images of Terra and Aqua. These satellites orbit in higher altitudes (~800 km) and use sensors with lower spatial resolution.

In order to examine the AFRI performance, it was first necessary to detect areas covered with smoke. There are, however, conditions under which this task is quite challenging. As mentioned previously, the identification of smoke in the African savannah region was difficult although the AERONET data clearly showed that the area of Mongu is smoke-contaminated. Fires are better spatially defined in images than smoke, therefore, they are usually used in order to detect and extrapolate smoke information (Kaufman *et al.* 1990). Fire monitoring may be achieved using MODIS's thermal bands.

However, active fires were also found to have an influence on the AFRI. Figures 3(*c*) and 7(*b*) are AFRI generated images of fire regions. In both figures one may see the protruding values of the pixels representing the active fire. The sensitivity of the index is derived from the proximity of the 2.1 μm wavelength to the thermal emission peak of the fire since the 2.1 μm channel is sensitive to fires (Kaufman *et al.* 1998). However, using the MODIS's thermal anomaly product

(MOD14) can easily solve this limitation by masking the pixels representing active fire.

The detection of smoke covered areas revealed differences in the smoke characteristics emitted by the savannah fires compared to the boreal forest fires. These differences can be explained by several reasons (Eck *et al.* 2001, Dubovik *et al.* 2002). The smaller particles and the three times more black carbon released to the atmosphere by savannah burning compared to forest burning (Andreae 1991), can be the result of differences in mode combustion (flaming versus smouldering), fuel type, and moisture content, and the ageing process of the aerosol. The savannah-origin particles create an overcast smoke over the region of fire, especially in areas with many fires as in Africa. Furthermore, due to the smaller size of the particles in the savannah fires, reflectance from these particles will be higher with shorter wavelengths. This may explain why savannah smoke is more difficult to notice than forest smoke in satellite images.

In addition to the different types of smoke, the performance of AFRI was examined over different vegetative covers as boreal forests, savannahs, and tropical forest using different images recorded by the MODIS sensor. The MODIS provides 44 different products, of which the fire product, the aerosol product, and the surface reflectance product were used in the current research. The latter undergoes atmospheric correction for gaseous absorption and molecular and aerosol scattering. The aerosol correction (MOD09) achieved only a partial success and many of the tested images included biomass-burning smoke. The AFRI may be used as an enhancer for aerosol correction.

The major limitation of the AFRI is waterbodies (and snow) due to the fact that the SWIR band (2.1 μm), which is used for calculating the index, is very sensitive to water due to the water's high absorption rate. Another limitation found in this research, is the smoke shadow. A very distinct shadow can be seen in the Rodeo–Chediski case study image (figure 1(*b*)). When observing the NDVI, EVI, and AFRI values of the cross-section pixels (figure 6) one can easily see the decrease in the VIs' values due to the shadow, similarly to the cloud shadow phenomenon. In order to eliminate these shadows from the image one may use a cloud-shadow mask procedure which can be found in the SPOT-VGT web site http://vegetation.cnes.fr/vgtprep/vgt2000/lissenscloud.pdf, although most of the procedures are developed for cloud shadow and there is a need to calibrate these masks in order to fit them to the smoke shadow.

Analysis of the MODIS instrument reconfirmed the strong correlation between the red and the SWIR wavelengths, allowing for highly successful computations of the AFRI. In all case studies the AFRI yielded high correlation with the NDVI over vegetated areas, but performed better under smoke conditions, as it succeeded to evaluate near-true vegetation condition through smoke, where the NDVI failed. Under smoke conditions AFRI also showed better results than the EVI although the latter is supposed to be an atmospheric resistance vegetation index.

5. Conclusions

- The AFRI index is proposed for monitoring vast areas of vegetation during periods of a smoke contaminated atmosphere. This has been illustrated on single images and on time series.

- The AFRI was found to be more efficient than the EVI for generating near-true vegetation condition values on images with smoke.
- The AFRI cannot be applied properly over waterbodies, snow, smoke shadow, and active fire.
- The MODIS sensor was found to be very useful for this research due to its relatively large number of bands, three different spatial resolutions, and a great number of relevant products.
- The AFRI should be further investigated on different kinds of vegetations in different regions of the world.
- The AFRI should be further investigated on smoke, volcanic ash, and industrial emissions with different levels of AOT.

References

ANDREAE, M.O., 1991, Biomass burning: its history, use, and distribution and its impact on environmental quality and global climate. In *Global Biomass Burning: Atmospheric, Climatic, and Biospheric Implications*, J.S. Levine (Ed), p. 569 (Cambridge: MIT Press).

BANNARI, A., MORIN, D., BONN, F. and HUETE, A.R., 1995, A review of vegetation indices. *Remote Sensing Reviews*, **13**, pp. 95–120.

DUBOVIK, O., HOLBEN, B., ECK, T.F., SMIRNOV, A., KAUFMAN, Y.J., KING, M.D., TANRÉ, D. and SLUTSKER, I., 2002, Variability of absorption and optical properties of key aerosol types observed in worldwide locations. *Journal of the Atmospheric Sciences*, **59**, pp. 590–608.

ECK, T.F., HOLBEN, B.N., WARD, D.E., DUBOVIK, O., REID, J.S., SMIRNOV, A., MUKELABAI, M.M., HSU, N.C., O'NEILL, N.T. and SLUTSKER, I., 2001, Characterization of the optical properties of biomass burning aerosols in Zambia during the 1997 ZIBBEE field campaign. *Journal of Geophysical Research*, **106**, pp. 3425–3448.

FERREIRA, L.G., YOSHIOKA, H., HUETE, A. and SANO, E.E., 2004, Optical characterization of the Brazilian Savanna physiognomies for improved land cover monitoring of the cerrado biome: preliminary assessments from an airborne campaign over an LBA core site. *Journal of Arid Environment*, **56**, pp. 3425–3447.

HOLBEN, B., VERMOTE, E., KAUFMAN, Y., TANRÉ, D. and KALB, V., 1992, Aerosol retrieval over land from AVHRR data - application for atmospheric correction. *IEEEE Transactions on Geoscience and Remote Sensing*, **30**, pp. 212–232.

HUETE, A., 1987, A soil-adjusted vegetation index (SAVI). *Remote Sensing of Environment*, **25**, pp. 295–309.

HUETE, A., DIDAN, K., MIURA, T., RODRIGUEZ, E.P., GAO, X. and FERREIRA, L.G., 2002, Overview of the radiometric and biophysical performance of the MODIS vegetation indices. *Remote Sensing of Environment*, **83**, pp. 195–213.

ISAACMAN, A., 2002, MODIS Level1B product data dictionary. Greenbelt, MD.

JUSTICE, C.O., GIGLIO, L., KORONTZI, S., OWENS, J., MORISETTE, J.T., ROY, D., DESCLOITRES, J., ALLEAUME, S., PETITCOLINN, F. and KAUFMAN, Y.J., 2002, The MODIS fire products. *Remote Sensing of Environment*, **83**, pp. 244–262.

KARNIELI, A., KAUFMAN, Y.J., REMER, L. and WALD, A., 2001, AFRI—aerosol free vegetation index. *Remote Sensing of Environment*, **77**, pp. 10–21.

KAUFMAN, Y.J., 1989, The atmospheric effect on remote sensing and its correction. In *Theory and Applications of Optical Remote Sensing*, G. Asrar (Ed), pp. 336–428 (New York: John Wiley).

KAUFMAN, Y.J. and REMER, L.A., 1994, Detection of forests using MID-IR reflectance - an application for aerosol studies. *IEEE Transactions on Geoscience and Remote Sensing*, **32**, pp. 672–683.

KAUFMAN, Y.J. and SENDRA, C., 1988, Algorithm for automatic atmospheric correction to visible and near-IR satellite imagery. *International Journal of Remote Sensing*, **9**, pp. 1357–1381.

KAUFMAN, Y.J. and TANRÉ, D., 1992, Atmospherically resistant vegetation index (ARVI) for EOS-MODIS. *IEEE Transactions on Geoscience and Remote Sensing*, **30**, pp. 261–270.

KAUFMAN, Y.J. and TANRÉ, D., 1996, Strategy for direct and indirect methods for correcting the aerosol effect on remote sensing: from AVHRR to EOS–MODIS. *Remote Sensing of Environment*, **55**, pp. 65–79.

KAUFMAN, Y.J., TUCKER, C.J. and FUNG, I., 1990, Remote sensing of biomass burning in the tropics. *Journal of Geophysical Research*, **95**, pp. 9927–9939.

KAUFMAN, Y.J., WALD, A., REMER, L., GAO, B., LI, R.R. and FLYNN, L., 1997a, The MODIS 2.1-mm channel. *IEEE Transactions on Geoscience and Remote Sensing*, **35**, pp. 1286–1298.

KAUFMAN, Y.J., KLIEDMAN, R.G. and KING, M.D., 1998, SCAR-B fires in the tropics: properties and remote sensing from EOS–MODIS. *Journal of Geophysical Research*, **102**, pp. 31 955–31 968.

KAUFMAN, Y.J., KARNIELI, A. and TANRÉ, D., 2000, Detection of dust over deserts using satellite data in the solar wavelengths. *IEEE Transactions on Geoscience and Remote Sensing*, **38**, pp. 525–531.

KING, M.D., KAUFMAN, Y.J., TANRÉ, D. and NAKAJIMA, T., 1999, Remote sensing of tropospheric aerosols from space: past, present, and future. *Bulletin of the American Meteorological Society*, **80**, pp. 2229–2259.

LIU, G.R., LIANG, C.K., KUO, T.H. and LIN, T.H., 2004, Comparison of the NDVI ARVI and AFRI vegetation index, along with their relations with the AOD using SPOT 4 vegetation data. *Terrestrial Atmospheric and Oceanic Sciences*, **15**, pp. 15–31.

MIURA, T., HUETE, A.R., VAN LEEUWEN, W.J.D. and DIDAN, K., 1998, Vegetation detection through smoke-filled AVIRIS images: an assessment using MODIS band passes. *Journal of Geophysical Research*, **103**, pp. 32 001–32 011.

QI, J., HUETE, A.R., MORAN, M.S., CHEHBOUNI, A. and JACKSON, R.D., 1993, Interpretation of vegetation indices derived from multi-temporal SPOT images. *Remote Sensing of Environment*, **44**, pp. 89–101.

ROUSE, J.W., HAAS, R.H., SCHELL, J.A., DEERING, D.W. and HARLAN, J.C., 1974, Monitoring the vernal advancement and retrogradation (greenwave effect) of natural vegetation. Final Report. NASA/GSFC, Greenbelt, MD, USA.

SLATER, P.N. and JACKSON, R.D., 1982, Atmospheric effects on radiation from soil and vegetation as measured by orbital sensors using various scanning directions. *Applied Optics*, **21**, pp. 3923–3931.

TOLLER, G.A. and ISAACMAN, A., 2002, MODIS Level1B product user's guide. Greenbelt, MD.

TUCKER, C.J., 1979, Red and photographic infrared linear combination for monitoring vegetation. *Remote Sensing of Environment*, **8**, pp. 127–150.

VERMOTE, E.F., EL SALEOUS, N.Z. and JUSTICE, C.O., 2002, Atmospheric correction of MODIS data in the visible to middle infrared: first results. *Remote Sensing of Environment*, **83**, pp. 97–111.